Efficient solar water splitting, exemplified by RuO2 catalyzed AlGaAs Si photoelectrolysis

ARTICLE · JANUARY 2000

Source: OAI

6 AUTHORS, INCLUDING:

Tetsuo Soga
Nagoya Institute of Technology
525 PUBLICATIONS **5,239** CITATIONS
SEE PROFILE

Masayoshi Umeno
Chubu University
580 PUBLICATIONS **8,133** CITATIONS
SEE PROFILE

Efficient Solar Water Splitting, Exemplified by RuO_2-Catalyzed AlGaAs/Si Photoelectrolysis

S. Licht,* B. Wang, and S. Mukerji

Chemistry Department, Technion, Haifa, 32000, Israel

T. Soga and M. Umeno

Nagoya Institute, Gokiso-Cho, Showa-ku, Nagoya 466, Japan

H. Tributsch

Hahn-Meitner-Institut, Abt. Solare Energetik, D-14109 Berlin, Germany

Received: June 8, 2000; In Final Form: July 27, 2000

Contemporary models are shown to significantly underestimate the attainable efficiency of solar energy conversion to water splitting, and experimentally a cell containing illuminated AlGaAs/Si RuO_2/Pt_{black} is demonstrated to evolve H_2 and O_2 at record solar driven water electrolysis efficiency. Under illumination, bipolar configured $Al_{0.15}Ga_{0.85}As$ ($E_g = 1.6$ eV) and Si ($E_g = 1.1$ eV) semiconductors generate open circuit and maximum power photopotentials of 1.30 and 1.57 V, well suited to the water electrolysis thermodynamic potential: $H_2O \rightarrow H_2 + {}^1/_2O_2$; $E^\circ_{H_2O} = E_{O_2} - E_{H_2}$; $E^\circ_{H_2O}(25\ ^\circ C) = 1.229$ V. The $E^\circ_{H_2O}$/photopotential matched semiconductors are combined with effective water electrolysis O_2 or H_2 electrocatalysts, RuO_2 or Pt_{black}. The resultant solar photoelectrolysis cell drives sustained water splitting at 18.3% conversion efficiencies. Alternate dual band gap systems are calculated to be capable of attaining over 30% solar photoelectrolysis conversion efficiency.

Introduction

Solar energy driven water splitting combines several attractive features for energy utilization. Both the energy source (sun) and the reactive media (water) are readily available and are renewable, and the resultant fuel (generated hydrogen) and the emission with fuel consumption (water) are each environmentally benign. Insolation (solar radiation) on semiconductors can generate significant electrical, electrochemical, or chemical energy.[1−3] Efficient solar driven water splitting requires a critical balance of the energetics of the solar conversion and solution phase redox processes. The UV and visible energy rich portion of the solar spectrum is transmitted through H_2O. Therefore, sensitization, such as via semiconductors, is required to drive the water-splitting process. In a solar photoelectrolysis system, the redox active interfaces can be in indirect or direct contact with the photosensitizer and comprise either an ohmic or Schottky junction. Independent of this interface composition, the various parameters in models predicting solar water splitting conversion efficiency, may be combined into two general parameters: (i) losses in optical energy conversion, η_{photo}, or (ii) losses in redox conversion of water to H_2 and O_2, $\eta_{electrolysis}$. Combined, these yield an overall solar electrolysis efficiency (excluding storage and utilization losses) as

$$\eta_{photoelectrolysis} = \eta_{photo}\eta_{electrolysis} \quad (1)$$

Early photoelectrolytic attempts used solution redox species such as $Ce^{3+/4+}$ and displayed poor quantum yields.[4] Further studies utilized semiconductors, such as TiO_2 (band gap, E_g, of 3.0 eV)[5] or $SrTiO_3$ ($E_g = 3.2$ eV).[6] The wide E_g excludes longer wavelength insolation, leading to poor efficiency. H_2 and O_2 evolution has been enhanced using large surface area or catalyst addition, but energy conversion efficiency remains low.[7] Early photolelectrolysis systems also combined p and n photoelectrodes.[8,9] A two or more band gap configuration can provide efficient matching of the solar spectra. p-InP and n-GaAs was demonstrated at 8.2% efficiency to generate H_2 and O_2.[10] More recently, a $GaInP_2$/GaAs photoelectrolysis cell was demonstrated at 12.4% efficiency.[11] Exposed semiconductors were modified to limit problematic photocorrosion.[12]

A limited fraction of incident solar photons have sufficient energy $> E_g$ to initiate charge excitation within a semiconductor. In stacked multijunction systems, the topmost cell absorbs (and converts) energetic photons but is transparent to lower energy photons. Subsequent layer(s) absorb the lower energy photons. In the solid state, such multiple band gap solar cells have achieved $\eta_{photo} > 30\%$.[1,13] In our recent model, the energetics of 12 distinct electrolytic multiple band gap solar cells were presented and comprise either Schottky or ohmic interfacial junctions, utilized either multiple or single photon events, and included pathways for electrochemical energy storage.[14] We have experimentally demonstrated several of these configurations at solar energy conversion efficiencies approaching 20%.[2,15]

Experimental Section

AlGaAs layers and a p-GaAs cap layer are grown sequentially by MOCVD on Si as previously described.[17−20] The bottom layer consists of a p^+-Si/n-Si/n^+-Si multijunction. Antireflection films are layers of MgF_2/ZnS. Au−Zn/Au and Au−Sb/Au are evaporated as contacts on p- and n-type electrodes. Solar

* To whom correspondence should be addressed. E-mail: chrlicht@techunix.technion.ac.il.

10.1021/jp002083b CCC: $19.00
Published on Web 09/01/2000

conversion efficiencies are calibrated using an AM solar simulator as previously reported,[20] and thereafter illumination is a 50 W tungsten−halogen lamp. IV characteristics were measured with a PINE AFCBP1 potentiostat (in a two-electrode configuration).

RuO_2 electrodes were prepared as described by ref 22. Ti (120 μm) foil is mechanically etched (sand blasted), then chemically etched with 20% HCl for 2 min, and water washed. Solvent was evaporated from 0.1 **M** $RuCl_3$ in 20% aqueous HCl and redissolved in a minimum volume of 2-propanol. Ti was then coated with $RuCl_3$ 2-propanol by brush and sintered 15 min at 350 °C. This coating is repeated five times and then 1 h annealed at 350 °C, producing a 2.3 μm thick RuO_2 layer on the substrate. Thicker or thinner coatings, or other annealing temperatures, resulted in higher ζ_{O_2}. For Pt_{black}, chloroplatinic acid was prepared with 3 g of H_2PtCl_6 and 0.25 g of $Pb(C_2H_3O_2)_2$ in 100 mL of water. Pt mesh (open area >60%, 30 × 30 mesh) was dilute nitric acid cleaned, water washed, and immersed in the chloroplatinic acid solution. A 5 min cathodic 4 V was applied, followed by 15 min electrolysis in 1 N H_2SO_4 removing chlorine impurities, and the solution was water washed. Analytical grade reagents and distilled, doubly deionized water were used throughout.

Results and Discussion

A bipolar semiconductor configuration comprises a two-photon/one-electron photoconversion process ($2h\nu \rightarrow e^-$), which can drive water electrolysis under the conditions in which the generated bipolar photovoltage, V_{photo}, is greater than the electrolysis potential, V_{H_2O}. A complex energetic challenge exists to choose bipolar band gaps with a combined maximum power point voltage tuned to V_{H_2O}, in a system also providing high η_{photo} (high fill factor, photopotential, and photocurrent). In the bipolar system, incident light first enters the wide band gap layer in which more energetic photons are absorbed; less energetic photons are transmitted. Absorbed wide band gap photons, $h\nu > E_{Gw}$, stimulate e^-/h^+pair excitation; a pn type or Schottky junction inhibits charge recombination driving charge into the small band gap layer, where further stimulation occurs by longer wavelength ($h\nu > E_{Gs}$) light. The subsequent junction facilitates charge transfer through the small band gap semiconductor. V_{photo} is the sum of the potentials of the individual band gap layers and is constrained to values less than $E_{Gw} + E_{Gs}$, by the saturation current, j_o, through Schottky or pn junctions. This yields a maximum power photopotential, V_{pmax}, less than 60% of the band gap in efficient devices:[16]

$$V_{photo}(j_{photo}) = V_w + V_s = (nkT/e)(\ln[1 + j_{photo}/j_{o-w}][1 + j_{photo}/j_{o-s}]) \quad (2)$$

$$V_{pmax} < 0.6(E_{Gw} + E_{Gs}) \quad (3)$$

To initiate electrolysis, V_{photo}, must be greater than V_{H_2O}. This study utilizes bipolar multijunction solid state layers; specifically a $Al_{0.15}Ga_{0.85}As$ (E_{Gw} = 1.6 eV), prepared on Si (E_{Gs} = 1.0 eV) as previously described.[17−20] Although of lower demonstrated efficiency than other dual band gap systems presented in Table 1, this AlGaAs/Si provides an effective example of a photopotential capable of efficiently driving a single electrolysis. Figure 1 presents the measured current/voltage characteristics for the AlGaAs/Si photocell at AM0 illumination. Further details and characterization of the cell are presented in ref 18. Under illumination, this bipolar cell generates an open circuit potential of 1.57 V, which is considerably larger the thermodynamic potential for the water splitting reaction. Also included are the photopotential dependence of solar to electrical conversion efficiency. A portion of the high η_{photo} domain lies at a potential above $E°_{H_2O}$ and in principle is sufficiently energetic to drive efficient photoelectrolysis.

TABLE 1: Predicted and Measured Photoelectrolysis Efficiencies[a]

photovoltaic	light level, sun	η_{photo}, % measd	$\eta_{photoelectrolysis}$, % pred max.	$\eta_{photoelectrolysis}$, % measd
GaInP/GaAs	1	30.3[1]	27−29[b]	
GaInP/GaAs	180	30.2[1]	27−29[b]	
GaAs/Si	350	29.6[1]	27−28[b]	
GaAs/GaSb	100	32.6[1]	29−31[b]	
InP/GaInAs	50	31.8[1]	29−30[b]	
GaAs/GaInAsP	40	30.2[1]	27−29[b]	
AlGaAs/Si	1	21.2[18]	19−20[b]	18.3 (S)
$GaInP_2$/GaAs	11			12.4[11]
InP/GaAs	1			8.2[10]

[a] Calculated $\eta_{photoelectrolysis}$ are from eq 13. [b] This study.

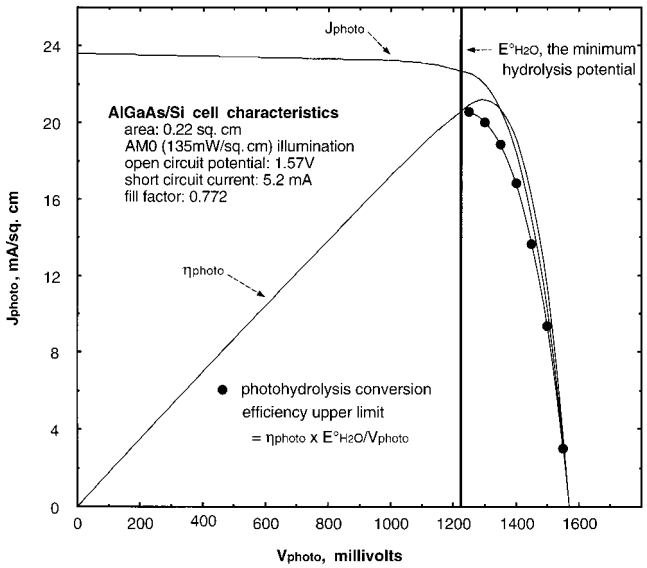

Figure 1. Current−voltage characteristics of the AlGaAs/Si cell at AM0 light intensity (135 mW/cm^2). η_{photo} = 100% × ($J_{photo}V_{photo}$)/$P_{illumination}$. Using the indicated, measured η_{photo} and V_{photo}, the upper limits of photohelectrolysis efficiency are calculated as $\eta_{photo} \times 1.229V/V_{photo}$.

The thermodynamic potential, $E°_{H_2O}$, for the water splitting reaction is given by

$$H_2O \rightarrow H_2 + {}^1/_2O_2$$
$$E°_{H_2O} = E°_{O_2} - E°_{H_2}; \quad E°_{H_2O}(25\ °C) = 1.229\ V \quad (4)$$

The subsequent challenge is to optimize sustained water electrolysis, without considerable additional energy losses. Effective water electrolysis must occur at a potential, V_{H_2O}, near the photocell point of maximum power. V_{H_2O} is greater than $E°_{H_2O}$ (=$-\Delta G_{H_2O}/nF$) due to overpotential losses, ζ, in driving an electrolysis current density, j, through both the O_2 and the H_2 electrodes:

$$V_{H_2O}(j) = E_{O_2}(j) - E_{H_2}(j) = (E°_{O_2} + \zeta_{O_2}(j)) - (E°_{H_2} + \zeta_{H_2}(j)) \quad (5)$$

Figure 2 summarizes $E_{O_2}(j)$ and $E_{H_2}(j)$, for several electrodes, including prepared Pt_{black} and RuO_2 prepared in accord with ref 21. Potentials were measured versus the gold oxide refer-

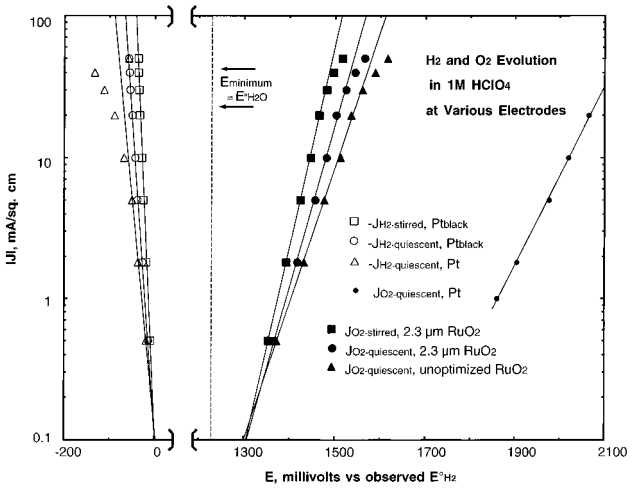

Figure 2. Potential variation with galvanostatic current density at various hydrogen or oxygen electrodes in 1 **M** $HClO_4$. Oxygen electrodes include 2.3 μm or unoptimized RuO_2 and Pt. Hydrogen electrodes are either Pt_{black} or planar Pt.

ence[22] but presented versus $E°_{H_2}$, from the observed $E°$ at Pt_{black}. As indicated by the figure's bold vertical line, this defines the minimum electrolysis potential as $\sim E°_{H_2O}$. Planar platinum and Pt_{black} are effective H_2 electrocatalysts. At low current densities (0.5 mA/cm^2), the observed Pt overpotential is low ($\zeta_{H_2} = -17$ mV), and even smaller ($\zeta_{H_2} = -13$ mV) with the Pt_{black} electrocatalyst, and smaller yet ($\zeta_{H_2} = -7$ mV) with a low level of convection (stirring) to improve mass transport and prevent observed gas buildup on the electrode surface.

Minimization of ζ_{O_2} is a greater challenge. In this case Pt is a poor electrocatalyst. ζ_{O_2} may be decreased $\sim$500 mV, utilizing an RuO_2 electrode (Figure 2). The kinetics of this effective oxygen electrocatalyst[21] have been attributed to catalysis by the intervening RuO_4/RuO_2 redox couple.[22,23] Unoptimized electrodes displayed higher ζ_{O_2} (Figure 2); these include electrodes prepared at higher annealing temperatures ($\geq$450 °C), or varying by 20% in thickness (from 2.3 μm). Using the 2.3 μm thick electrodes, at 0.5 mA/cm^2, convection decreased the observed oxygen evolution potential from 1.37 to 1.35 V. These reproducible potentials are marginally better than predicted by the 1.38 V RuO_4/RuO_2 rest potential but are consistent with expected intermediate valence oxides (including RuO_4^- and RuO_4^{2-}) and interfacial activity deviations.

In the absence of competing redox couples, the faradaic efficiency of H_2 and O_2 evolution approaches 100%, and $\eta_{electrolysis}$ is determined by the current-limited $V_{H_2O}(j)$:

$$\eta_{electrolysis} = E°_{H_2O}/V_{H_2O}(j)$$

$$\eta_{electrolysis}(25\ °C) = 1.229\ V/V_{H_2O}(j) \quad (6)$$

The Figure 3 inset contains the eq 6 determined $\eta_{electrolysis}$. The limiting maximum $\eta_{photoelectrolysis}$ can be readily determined from the solar to electrical conversion efficiency. Expanding eq 1 with eq 6, $\eta_{photoelectrolysis}$ is diminished from η_{photo} by the potential of the stored energy compared to the potential at which the water electrolysis occurred:

$$\eta_{photoelectrolysis}(T) = \frac{\eta_{photo}(T)\, E_{H_2O}(T)}{E_{O_2}(T) - E_{H_2}(T)}$$

$$\eta_{photoelectrolysis}(25\ °C) = \frac{1.229\ V \times \eta_{photo}}{V_{H_2O}} \quad (7)$$

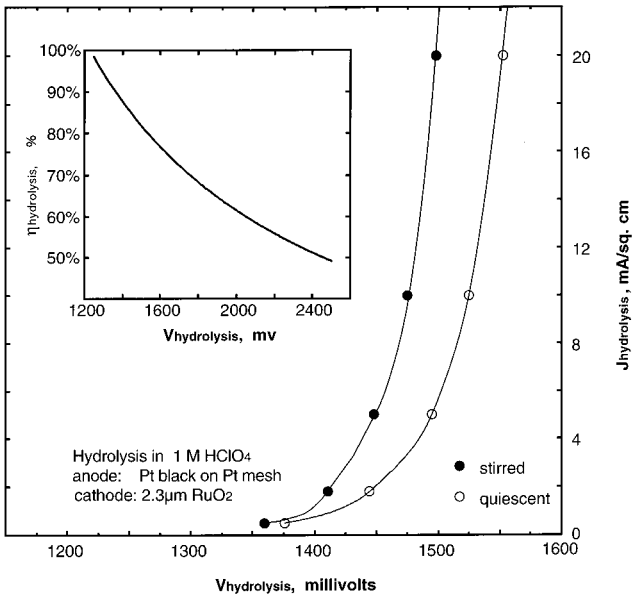

Figure 3. Measured variation of the V_{H_2O} with current density in 1 M $HClO_4$, using equal area 2.3 μm RuO_2 and Pt_{black}. Inset: Calculated η_{photo}, in a 100% faradaic efficient process, as a function of V_{H_2O}.

Figure 1 includes these limiting $\eta_{photoelectrolysis}$ values for our AlGaAs/Si system determined from our measured values of η_{photo} at various values of V_{photo}. AlGaAs/Si solar photoelectrolysis at conversion efficiencies exceeding 20% (Figure 1) are, in principle, possible at potentials approaching the E_{H_2O} limit. The main portion of Figure 3 presents the water electrolysis potential, V_{H_2O}, determined under stirred or quiescent conditions and measured in 1 M $HClO_4$ using equal areas of the optimized RuO_2 and Pt_{black} electrodes. These measurements of the electrolysis current, as a function of potential, enable us to predict the AlGaAs/Si photocurrent at which photoelectrolysis will occur.

Our photoelectrolysis cell consists of illuminated AlGaAs/Si RuO_2/Pt_{black} electrolysis. With these active electrocatalysts, high values of $\eta_{electrolysis}$ are ensured by using large surface areas of the electrolysis electrodes, compared to the illuminated area. This is accomplished without increasing the illuminated electrode area, as schematically represented in Figure 4a, by utilizing a large vertical depth of electrolysis electrodes compared to the cross section of illumination. Specifically, the 10 cm^2 Pt_{black} and RuO_2 electrodes utilized are large compared to the 0.22 cm^2 illuminated area and chosen such that at Figure 1 photopotentials of 1.3−1.4 V, the photocurrent of 4.1−4.8 mA equates to a electrolysis j < 0.5 mA/cm^2. In Figure 4b is the H_2 and O_2 electrolysis current generated by this cell as a function of time. The average photocurrent of 4.42 mA (generating a current density of 20.1 mA/cm^2 at the illuminated electrode area, and 0.44 mA/cm^2 at the electrolysis electrodes) corresponds to a photopotential of 1.36 V in Figure 1, comparable to the equivalent electrolysis potential at 0.5 mA/cm^2 in Figure 3. The overall efficiency is determined by the 1.229 V energy stored as H_2 and O_2 and the incident photopower (135 mW/cm^2):

$$\eta_{photoelectrolysis} = 100\% \times 20.1\ mA/cm^2 \times 1.229\ V/135\ mW/cm^2 = 18.3\% \quad (8)$$

In eq 1, the significance of the electrolysis, compared to photo, components of the conversion efficiency is evident upon analysis of a recent report of a 12.4% photoelectrolysis cell. The cell contained a Pt-coated $GaInP_2$ hydrogen electrode in

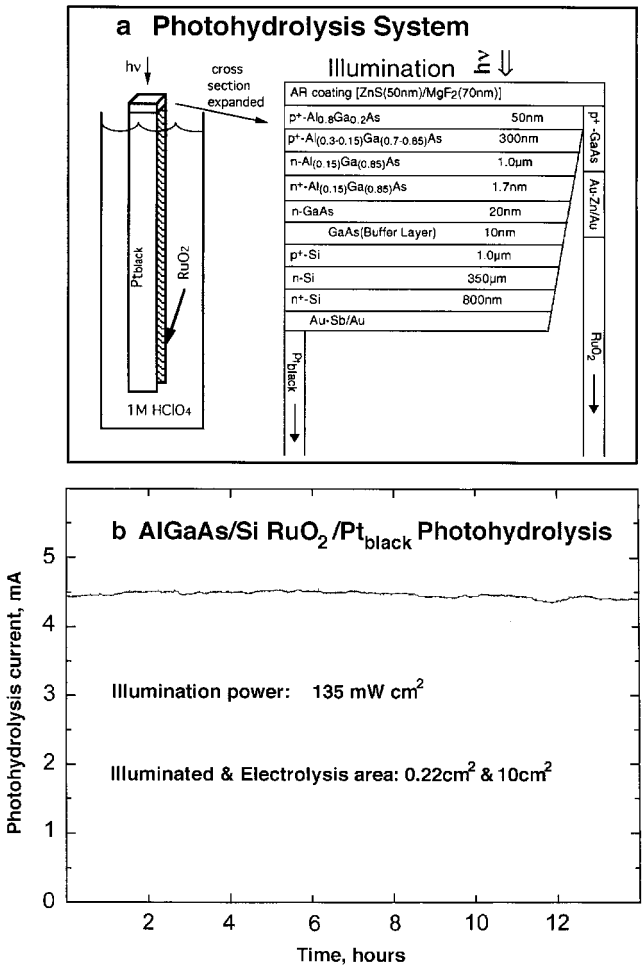

Figure 4. Schematic representation (a) and measured characteristics (b) of the illuminated AlGaAs/Si RuO_2/Pt_{black} photoelectrolysis cell. Further details of the layered AlGaAs/Si structure are given in ref 18.

bipolar contact with a GaAs junction driving an oxygen electrode.[11] Consistent with extrapolation of the leftmost curve of Figure 2, at their specified 11 sun illuminated electrolysis current density of 120 mA/cm^2, ζ_{H_2} will exceed 300 mV at Pt. Oxygen losses will be even larger, and the cell will have a total overpotential loss >700 mV. Two such cells will have losses $> E^\circ_{H_2O}$, unnecessary losses if the cell was illuminated at 1 sun, or employed a larger surface area or more effective electrocatalysts. Under these conditions, two $GaInP_2$/GaAs cells placed in series should drive three water electrolysis cells in series, effectively increasing the relative photoelectrolysis efficiency by 50%.

Thermodynamic heat considerations can be applied to photoconversion. Some heat, Q, will always be lost due to charge carrier relaxation and vibrations. This heat difference will involve an entropy turnover $Q/T = \Delta S$. Photoenergy conversion efficiencies can be optimized by minimizing ΔH_{ph}. For band gap excitation ΔH_{ph} will correspond to E_g. If the absorbed photon energy is much higher than E_g, then ΔH_{ph} is correspondingly higher. If E_g is much larger than the required electrolysis energy, ΔG_{H_2O}, then the predicted efficiency will be low. The efficiency will be higher, the better the photovoltaic system is matched to the chemical one. Consequently, there will be a thermodynamic photoefficiency describing the generation of electrochemical free energy for electrolysis:

$$\eta_{photo} = \Delta G_{H_2O}/\Delta H_{ph} \tag{9}$$

In reality, how small can ΔH_{ph} be made, as compared to ΔG_{H_2O}? For photosynthesis it has been estimated that of the 1.8 eV excitation energy of chlorophyll, at least 0.6−0.8 eV are lost before the energy can be stored in stable chemical products. Photosynthesis, however, requires many subsequent electron-transfer steps, which all will contribute to efficiency losses. The molecules involved are also complicated and quite unstable compounds maintained through self-organization. Photoelectrolysis systems with many fewer components, and with fewer degrees of freedom in terms of chemical reactivity, can better approach the ideal energy conversion efficiency. As with the opposite case when fuel is consumed to produce power (resulting in a fuel cell with efficiency $\Delta G/\Delta H$) the optimal efficiency for electrolysis must include entropy considerations and will strongly depend on the temperature-dependent enthalpy change ($\Delta H_{H_2O}(T)$):

$$\eta_{electrolysis-opt} = \Delta H_{H_2O}/\Delta G_{H_2O} \tag{10}$$

Practical electrolysis has to include losses so that the efficiency becomes

$$\eta_{electrolysis} = \Delta H_{H_2O}/(\Delta G_{H_2O} + \text{losses}) \tag{11}$$

A thermoneutral potential, E_{tn} ($E_{tn} = \Delta H_{H_2O}/zF$), is defined where no heat turnover is observed is $E_{tn} = 1.48$ V for water electrolysis.[24] If, due to effective catalysis, the total electrolysis cell voltage is close to 1.48 V, one approaches $\eta_{electrolysis} \approx 1$.

If we return to eq 1 and substitute eqs 9 and 11, we obtain

$$\eta_{photoelectrolysis} = \eta_{photo}\eta_{electrolysis} = \Delta H_{H_2O}/\Delta H_{ph}(1 + \text{losses}/\Delta G_{H_2O}) \tag{12}$$

Two conclusions arise from eq 12. First it is seen that efficiency can be maximized, if electrochemical "losses" can be made small as compared to the Gibbs free energy change for water electrolysis, ΔG_{H_2O}. Second it is seen that ΔH_{H_2O}, the enthalpy of water electrolysis (with little temperature dependence), is involved in determining the overall efficiency as well as ΔH_{ph}, the enthalpy of photogenerated charge carriers. If these two can properly be matched, a maximum overall efficiency may be accomplished.

The principal solar water splitting models[3,25] predict similar dual band gap photoelectrolysis efficiencies of only 16% and 10−18%, respectively. Each are lower than our observed water splitting efficiency. The physics of these models were superb, but their analysis was influenced by dated technology and underestimated the experimental η_{photo} attained by contemporary devices, or underestimated the high experimental values of $\eta_{electrolysis}$ that can be attained. For example, Bolton et al. estimates low values of η_{photo} (less than 20% conversion) due to assumed cumulative relative secondary losses, which include 10% reflection loss, 10% quantum-yield loss, and 20% absorption loss. As summarized in Table 1, demonstrated η_{photo} are substantially higher than 20%. Many η_{photo} that have been carefully reviewed or monitored are in excess of 30%.[1]

Each of the cells in the Table 1 exhibits an open circuit photopotential significantly greater than the minimum potential necessary to split water. The majority of these cells can generate a photopotential in excess of 2 V. An unnecessary limit of one multiple band gap photoexcitation per electrolysis would underutilize V_{photo}, diminishing $\eta_{electrolysis}$. For example a GaInP/GaAs cell has a maximum power photopotential of 2.0−2.1 V and an open circuit potential of 2.3 V.[26] Two such cells in series will efficiently drive three 1.3−1.4 V water electrolysis cells

in series. This paper has demonstrated water electrolysis at 1.36 V (Figure 3 inset) and electrolysis efficiencies of over 90%. It is reasonable that with larger surface area, or more effective electrocatalysis, these efficiencies will approach 95%. Using this range of $\eta_{\text{electrolysis}} = 90-95$

$$\eta_{\text{photoelectrolysis}}(\text{predicted maximum}) = \eta_{\text{photo}} \times 90-95\% \quad (13)$$

Table 1 includes predicted maximum $\eta_{\text{photoelectrolysis}}$ using observed η_{photo} of various dual band gap sensitizers. It is seen that solar water splitting efficiencies may be viable at up to double the amount of that previously predicted. Efficient, three or more multiple band gap, photoelectrolysis will be expected to be capable of attaining even higher efficiencies.

In this study, the attainable levels of solar driven electrolysis, to generate H_2 and O_2, are shown to be considerably higher than generally recognized. New experimental and calculated high levels of solar water splitting can provide impetus to the development of hydrogen as a solar generated, renewable and clean, fuel.

Acknowledgment. We thank support by the BMBF Israel-German Cooperation, the Belfer Energy Foundation, and the Berman-Shein Solar Fund.

References and Notes

(1) Green, M. A.; Emery, K.; Bucher, K.; King, D. L.; Igari, S. *Prog. Photovolt*. **1999**, *11*, 31.
(2) Licht, S.; Wang, B.; Soga, T.; Umeno, M. *Appl. Phys. Lett*. **1999**, *74*, 4055.
(3) Bolton, J. R.; Strickler, S. J.; Connolly, J. S. *Nature* **1985**, *316*, 495.
(4) Heidt, L. J.; McMillan, A. F. *Science* **1953**, *117*, 75.
(5) Fujishima, A.; Honda, K. *Nature* **1972**, *238*, 37.
(6) Bolts, J. M.; Wrighton, M. S. *J. Phys. Chem*. **1976**, *80*, 2641.
(7) Memming, R. *Top. Curr. Chem.* **1988**, *143*, 79.
(8) Nozik, A. *Appl. Phys. Lett*. **1976**, *29*, 150.
(9) White, J.; Fan, F.-R.; Bard, A. J. *J. Electrochem. Soc*. **1985**, *132*, 544.
(10) Kaintala, R. C.; Bockris, J. O'M. *Int. J. Hydrogen Energy* **1988**, *13*, 375.
(11) Khaselev, O.; Turner, J. *Science* **1998**, *280*, 425.
(12) Bogandoff, P.; Friebe, P.; Alonso-Vante, N. *J. Electrochem. Soc*. **1998**, *145*, 576.
(13) Licht, S. *Interface* **1997**, *6*, 34.
(14) Licht, S.; Khaselev, O.; Soga, T.; Umeno, M. *Electrochem. Solid State Lett*. **1998**, *1*, 20.
(15) Licht, S.; Khaselev, O.; Ramakrishnan, P. A.; Soga, T.; Umeno, M. *J. Phys. Chem*. **1998**, *102*, 2536; *ibid*, 2546.
(16) Memming, R. In *Photochemical Conversion and Storage of Solar Energy*; Pelizzetti, E., Schiavello, M., Eds.; Kluwer Academic Publishers: Netherlands, 1991; pp 193-212.
(17) Soga, T.; Umeno, M.; Jimbo, T. *J. Appl. Phys*. **1996**, *79*, 9375. Soga, T.; Kato, T.; Yang, M.; Umeno, M.; Jimbo, T. *J. Appl. Phys*. **1995**, *78*, 4196.
(18) Soga, T.; Baskar, K.; Kato, T.; Jimbo, T.; Umeno, M. *J. Cryst. Growth* **1976**, *174*, 579.
(19) Soga, T.; Yang, M. T.; Jimbo, T.; Umeno, M. *Jpn. J. Appl. Phys*. **1998**, *35*, 1401.
(20) Umeno, M.; Egawa, T.; Soga, T.; Jimbo, T. *Solar Energy Mat*. **1996**, *41/42*, 395.
(21) Lodi, G.; Sivieri, E.; Debattisti, A.; Trasatti, S. *J. Appl. Electrochem*. **1978**, *8*, 135.
(22) Alonso-Vante, N.; Colell, H.; Stimming, U.; Tributsch, H. *J. Phys. Chem*. **1993**, *97*, 7381.
(23) Salvador, P.; Alonso-Vante, N.; Tributsch, H. *J. Electrochem. Soc*. **1998**, *145*, 216.
(24) Gutman, F.; Murphy, O. J. In *Modern Aspects of Electrochemistry*; White, R. E., Bockris, J. O'M., Conway, B. E., Eds.; Plenum: New York, 1983; p 5.
(25) Weber, M. F.; Digman, M. J. *Int. J. Hydrogen Energy* **1986**, *11*, 225. ibid, *J. Electrochem. Soc*. **1984**, *131*, 1258.
(26) Friedman, D. J.; Kurtz, S. R.; Bertness, K.; Kibbler, A. E.; Kramer, C.; Olsen, J. M. *Prog. Photovolt*. **1995**, *3*, 47.